PROCEEDINGS OF SCIENCE

Potential of the Askaryan Fraction of the Radio Emission from Cosmic-ray Air Shower for X_{max} Reconstruction

Ek Narayan Paudel,[a,*] **Alan Coleman**[a] **and Frank Schröder**[a,b]

[a] *University of Delaware, Department of Physics and Astronomy, Bartol Research Institute Newark, Delaware, USA*

[b] *Institute for Astroparticle Physics, Karlsruhe Institute of Technology, Karlsruhe, Germany*

E-mail: narayan@udel.edu, alanc@udel.edu, fgs@udel.edu

There is an ongoing effort to improve the sensitivity of the IceTop surface array at the South Pole by the addition of surface radio antennas. With a simulation study, we investigated the dependencies of the Akaryan relative to the geomagnetic emission in the band of 70-350 MHz at the South Pole. We used CoREAS to simulate the radio emission from cosmic ray air showers at that location using a star-shape pattern and used the polarization of the radio emission on the ground to calculate the relative Askaryan fraction at the Cherenkov ring of the radio footprint. We then investigated the dependence of the Askaryan fraction on several shower parameters, among them, the distance to the shower maximum ($d_{X_{\rm max}}$). Based on the finding, we have developed a model that uses the average fraction as well as the shower geometry to reconstruct the mass-sensitive depth of shower maximum ($X_{\rm max}$) for a given atmosphere. The theoretically achievable precision can compete with other methods for $X_{\rm max}$ measurement by radio arrays. Therefore, the Askaryan fraction - or more generally - the polarization of the radio signal may serve as an additional input for future multivariate approaches of $X_{\rm max}$ reconstruction.

9th International Workshop on Acoustic and Radio EeV Neutrino Detection Activities - ARENA2022
7-10 June 2022
Santiago de Compostela, Spain

*Speaker

PoS(ARENA2022)047

1. Introduction

The method of using radio emission from air showers to detect cosmic rays has developed into an effective technique, more so if used in combination with other air shower detectors. [1, 2]. Radio emission from cosmic-ray air showers is mainly geomagnetic in nature. It is produced by the separation of charged particles in the electromagnetic component of an air shower in the geomagnetic field. This is illustrated in the left half of fig. 1. In addition, there is radially polarized Askaryan emission produced by the a time-varying negative charge excess that accumulates in the air shower front as shown in the right half of fig. 1. When observed in the shower plane, geomagnetic emission is linearly polarized along the direction of Lorentz force[1], and Askaryan emission is radially polarized. Hence, the radio footprint measured at the ground will be the superposition of these two emissions differing in magnitude and polarization. Among other factors, the signal detected by the radio antennas depends on the geometry of the air shower relative to the Earth's magnetic field and antenna location in the radio footprint.

IceTop, the surface detector of the IceCube Neutrino observatory [4, 5] at the South Pole is planned to be enhanced using elevated scintillators and radio antennas. This motivated the present simulation study of the radio emission from air showers in the band of 70 – 350 MHz for the location of the South Pole. We use the polarization of the simulated radio emission to extract the geomagnetic and the Askaryan contributions. We also study the dependence of the relative Askaryan fraction on various air-shower parameters and its potential use for the reconstruction of X_{max}.

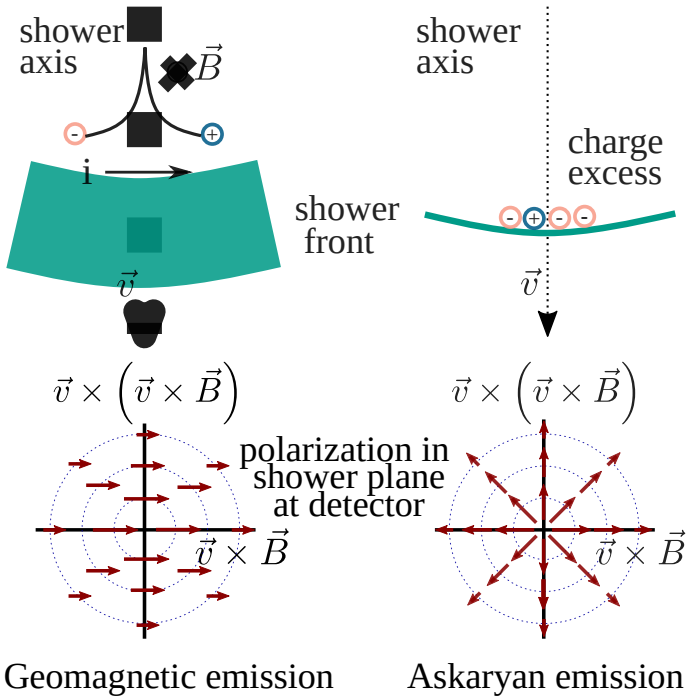

Zenith angle (θ)	$\leq 71.5°$
Energy	$10^{17.0}$ - $10^{17.1}$
Hadronic interaction model	Fluka2011, SIBYLL2.3d
Atmosphere	April South Pole atmosphere (ATMOD = 33)
Observation level	2840 m above sea level
Geomagnetic field ($\lvert\vec{B}\rvert$)	54.58 µT at 17.87° inclination
Thinning	$10^{-6.0}$

Table 1: Specifications used in air shower simulations.

2. Simulation of the radio emission from air shower at the South Pole

When an energetic primary cosmic ray enters the Earth's atmosphere, it interacts with air molecules and generates an extensive air shower. The radio emission from such air showers is simulated using CORSIKA with its CoREAS add-on [6, 7]. We simulated 1800 showers each of proton and iron primaries for the South Pole location with specifications listed in table 1. We used a star-shaped antenna pattern having eight spokes with 20 sampling points each for the simulation of the radio signal on ground (see Figure 2 for an example). Figure 3 shows example traces of the simulated radio signal filtered in the frequency bandwidth of 70-350 MHz.

We used the following signal-to-noise ratio (SNR) for a quality cut of the simulated traces:

$$\mathrm{SNR} = \left(\frac{S_{peak}}{N_{RMS}}\right)^2, \tag{1}$$

where S_{peak} is the peak of the Hilbert envelope of the signal trace and N_{RMS} is the root mean square of the last 40 % of the waveform. A cut of SNR > 10^4 was applied to remove incoherent signals and artifacts of thinning during CORSIKA simulations.

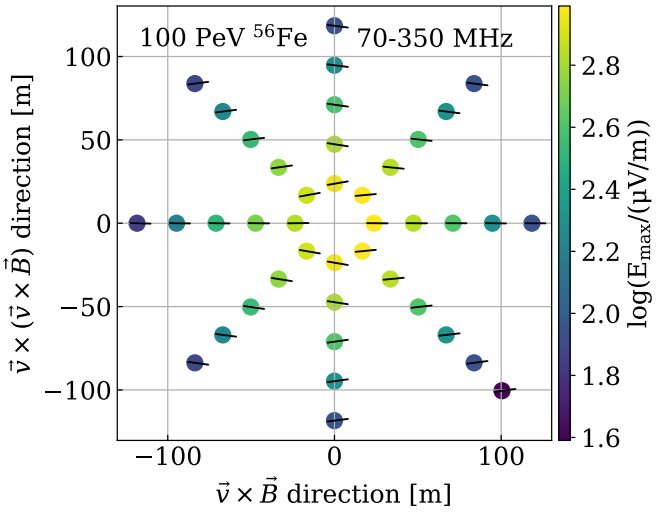

Figure 2: Radio footprint on a star-shape antenna pattern for a 100 PeV vertical iron shower. The polarization plane of the electric field at the signal peak is shown by the orientation of the line at each antenna location.

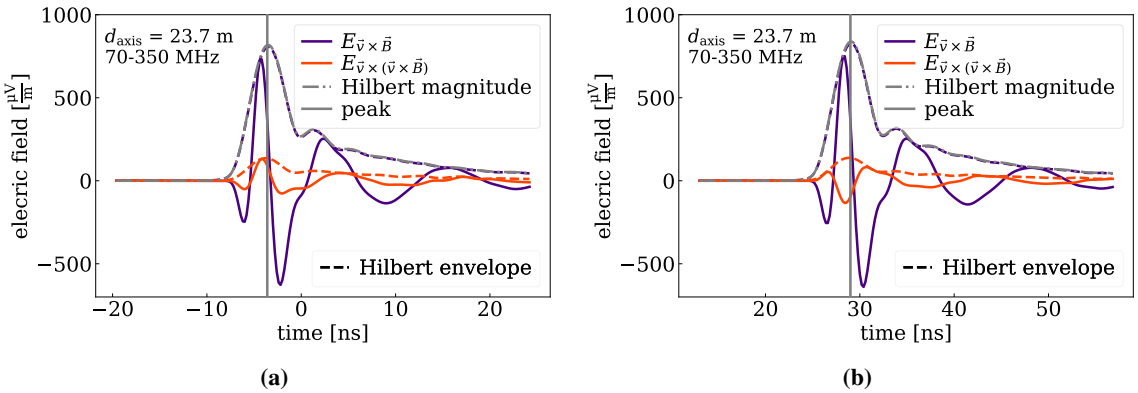

Figure 3: Simulated radio signal for a location along the (a) positive and (b) negative $\vec{v} \times (\vec{v} \times \vec{B})$ axis.

Again, most of the radio emission from the cosmic ray air shower is produced from the region close to the shower maximum. Therefore, the radio emission measured at the ground level has the signature of where in the atmosphere the emission originated and can reveal the location of the shower maximum. Figure 4 shows the conceptual representation of the radio emission from of an air shower.

Figure 5 shows the distribution of the true X_{max} for proton and iron initiated air showers of energy $10^{17.0}$ – $10^{17.1}$ eV. Iron showers have in general a smaller mean value and spread of X_{max} than proton showers. Hence, measurement of X_{max} gives us a tool to estimate the mass composition

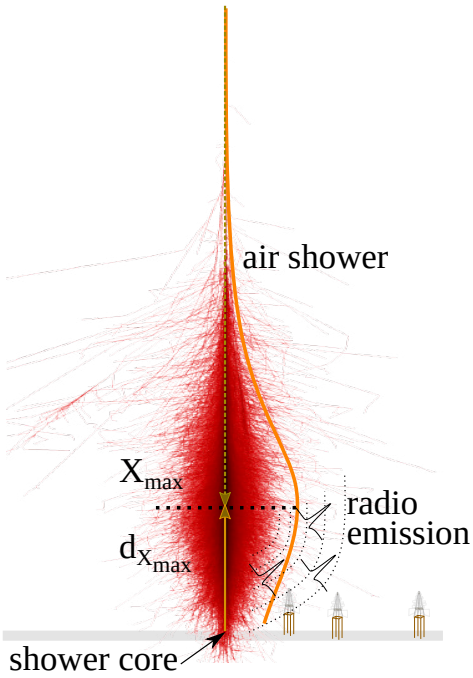

Figure 4: Sketch of a cosmic-ray air shower and its radio emission. Most of the radio emission occurs from the region close to shower maximum, X_{max}, and can be detected by radio antennas on the ground.

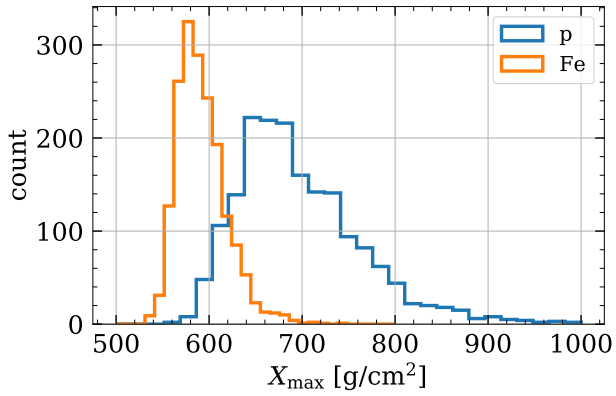

Figure 5: X_{max} distribution of simulated proton and iron showers of $10^{17.0}$ – $10^{17.1}$ eV at the South Pole.

of the primary cosmic rays.

3. Relative Askaryan fraction

To calculate the strengths of the Askaryan relative to the geomagnetic emission, as a first step, the simulated electric field at each location in the star-shape pattern is transformed to the shower plane perpendicular to the shower axis v, with the $\vec{v} \times \vec{B}$ and $\vec{v} \times (\vec{v} \times \vec{B})$ directions as axes. As apparent from the lower panel in fig. 1, the geomagnetic and Askaryan components are perpendicular to each other along the $\vec{v} \times (\vec{v} \times \vec{B})$ axis. Hence, we quantify the relative Askaryan fraction as

$$a_{\text{rel}} \equiv \sin \alpha \left(\frac{A}{G} \right). \tag{2}$$

where α is the angle between the geomagnetic field and the shower direction, and A and G represent the amplitude of Askaryan and geomagnetic emission determined as the peak of the Hilbert envelope of the respective polarization component at each antenna location along the $\vec{v} \times (\vec{v} \times \vec{B})$ axis.

As a_{rel} varies with the distance to the shower axis (see fig. 6), a distance window based on the Cherenkov ring can be used to characterize each shower by its average relative Askaryan fraction

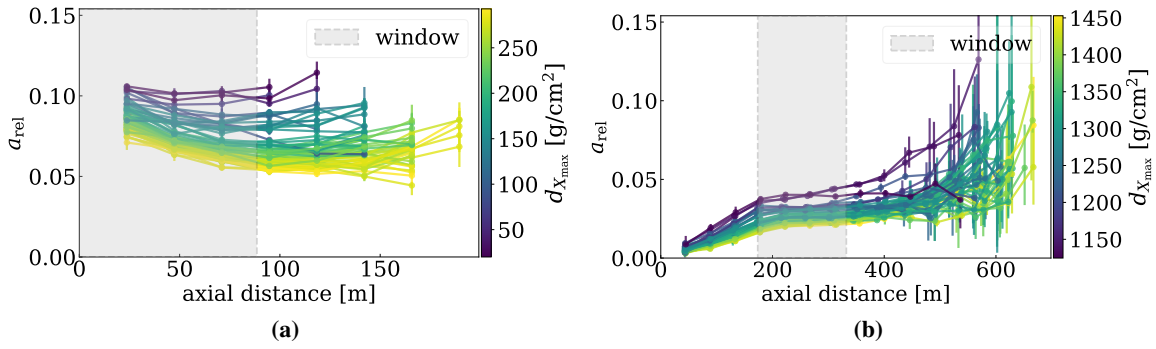

Figure 6: Relative Askaryan fraction (a_{rel}) over the distance from the shower axis for θ (a) 35°-36° and (b) 69°-70°. Mean values are connected by lines to guide the eye. The color code indicates the distance to the shower maximum ($d_{X_{max}}$). In a window based on the location of the Cherenkov ring a_{rel} is relatively stable.

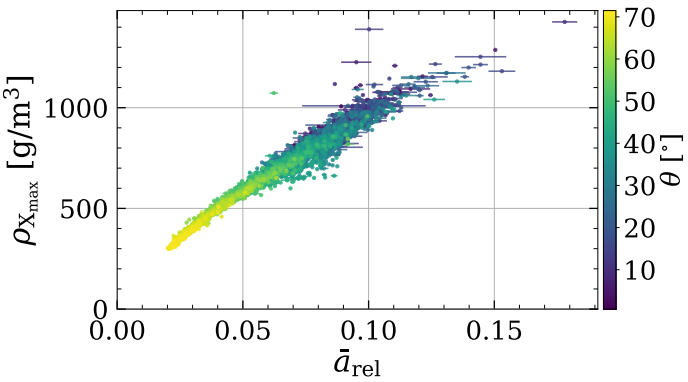

Figure 7: Density at X_{max}, $\rho_{X_{max}}$, over the average relative Askaryan fraction, $\bar{a}_{rel}$. The color bar represent the zenith angle of the shower. Showers with lower zenith angle tend to have a lower geomagnetic radio emission (due to the geomagnetic inclination of only 17.87°), and hence a larger Askaryan fraction, and also tend to have the shower maximum in the denser region deep in the atmosphere.

($\bar{a}_{rel}$) within the window [8]. a_{rel} also varies as a function of distance to the shower maximum ($d_{X_{max}}$) as is seen from the color axis in fig. 6.

4. Dependence of $\bar{a}_{rel}$ on shower parameters

When the atmospheric density at the shower maximum, $\rho_{X_{max}}$, is plotted over the average Askaryan fraction $\bar{a}_{rel}$ in fig. 7, it can be seen that $\rho_{X_{max}}$ has a clear dependence on $\bar{a}_{rel}$ as noted previously in [9]. We further studied the dependence of $d_{X_{max}}$ with $\bar{a}_{rel}$. As seen in fig. 8, $d_{X_{max}}$ has a strong dependence on the reciprocal of the Askaryan fraction, $\frac{1}{\bar{a}_{rel}}$, and on the zenith angle θ. We

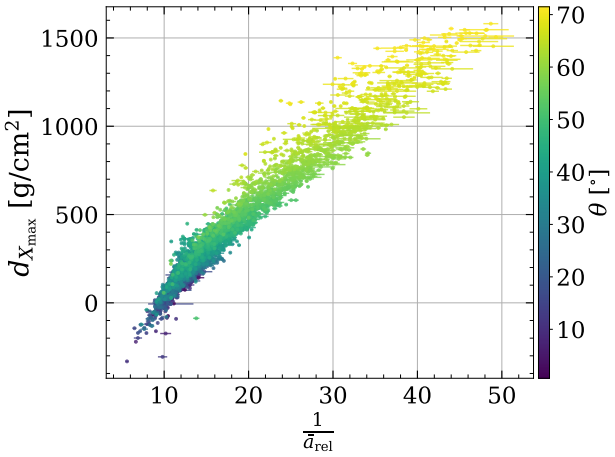

Figure 8: Distance to X_{max}, $d_{X_{max}}$, as function of the reciprocal of the Askaryan fraction, $\frac{1}{\bar{a}_{rel}}$, for proton and iron showers of primary energy $10^{17.0}$ – $10^{17.1}$ eV. The color bar represents the zenith angle θ (from [8]).

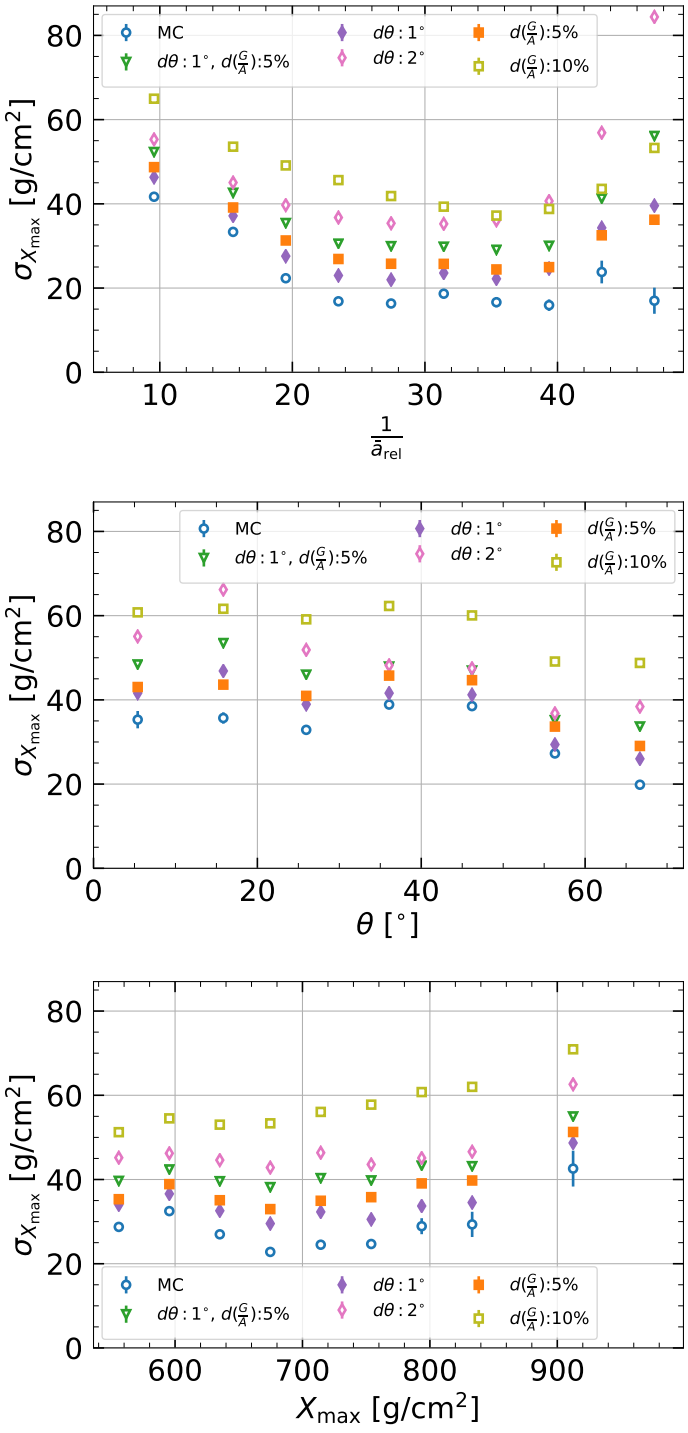

Figure 9: Theoretically predicted resolution of X_{max} as a function of $\frac{1}{\bar{a}_{rel}}$, θ, and X_{max}. The ideal case without any experimental uncertainty is represented by blue circles. 1° and 2° arrival direction uncertainty is included in purple and pink diamonds. Similarly, 5 % and 10 % measurement uncertainty of $\frac{G}{A}$ is reflected by the orange and green squares. Finally, the combined inclusion of 1° angular uncertainty and 5 % uncertainty in $\frac{G}{A}$ is represented by the green triangles (from [8]).

describe these dependencies of $d_{X_{max}}$ using the following equation with parameters a to h [8]:

$$d_{X_{max}} = \begin{bmatrix} 1 & \frac{1}{\bar{a}_{rel}} & \left(\frac{1}{\bar{a}_{rel}}\right)^2 & \left(\frac{1}{\bar{a}_{rel}}\right)^3 \end{bmatrix} \begin{bmatrix} a & b \\ c & d \\ e & f \\ g & h \end{bmatrix} \begin{bmatrix} 1 \\ \sec\theta \end{bmatrix}. \tag{3}$$

X_{max} can be obtained from $d_{X_{max}}$ for a given atmosphere. Hence, eq. (3) can be used to reconstruct X_{max} from measurements of $\frac{1}{\bar{a}_{rel}}$ and θ. The theoretically expected resolution of X_{max} is plotted in fig. 9 for different scenarios. If the true values of θ and fraction $\frac{G}{A}$ are known, the resolution provided by eq. (3) is about 16 - 42 g cm^{-2}. The resolution gets worse when we include an angular uncertainty of 1° or 2°. The resolution also worsens when an uncertainty of 5 % or 10 % for $\frac{G}{A}$ is included. Assuming both, 1° angular uncertainty and 5 % uncertainty on $\frac{G}{A}$, the X_{max} resolution is about 29 - 55 g cm^{-2}.

5. Conclusion

We separated the geomagnetic and Askaryan components of the radio emission from air showers simulated with CoREAS for the South Pole using polarization information. We identified a distance window based on the Cherenkov ring to calculate the average relative Askaryan fraction characteristic for an air shower and studied its dependencies on various air-shower parameters like $d_{X_{max}}$, θ, and $\rho_{X_{max}}$. To test the utility of using the strong dependence of $d_{X_{max}}$ on $\frac{1}{\bar{a}_{rel}}$ and θ, we developed a parametrization of $d_{X_{max}}$ as function of $\frac{1}{\bar{a}_{rel}}$ and sec θ and studied the resolution of the mass-sensitive shower parameter X_{max} that can be achieved considering various measurement uncertainties. The best achievable resolution of X_{max} reconstruction is about 16 - 42 g cm^{-2}. If we include 1° angular uncertainty and 5 % uncertainty of the ratio $\frac{G}{A}$, the resolution is in the range of about about 29 - 55 g cm^{-2}.

References

[1] T. Huege, *Radio detection of cosmic ray air showers in the digital era*, *Phys. Rept.* **620** (2016) 1 [1601.07426].

[2] F.G. Schröder, *Radio detection of Cosmic-Ray Air Showers and High-Energy Neutrinos*, *Prog. Part. Nucl. Phys.* **93** (2017) 1 [1607.08781].

[3] C.W. James, *Nature of radio-wave radiation from particle cascades*, *Phys. Rev. D* **105** (2022) 023014 [2201.01298].

[4] IceCube collaboration, *The IceCube Neutrino Observatory: Instrumentation and Online Systems*, *JINST* **12** (2017) P03012 [1612.05093].

[5] IceCube collaboration, *IceTop: The surface component of IceCube*, *Nucl. Instrum. Meth. A* **700** (2013) 188 [1207.6326].

[6] D. Heck et al., *Report FZKA 6019, Forschungszentrum Karlsruhe*, 1998.

[7] T. Huege, M. Ludwig and C.W. James, *Simulating radio emission from air showers with CoREAS*, *AIP Conf. Proc.* **1535** (2013) 128 [1301.2132].

[8] E.N. Paudel, A. Coleman and F.G. Schroeder, *Simulation study of the relative Askaryan fraction at the south pole*, *Phys. Rev. D* **105** (2022) 103006 [2201.03405].

[9] C. Glaser, M. Erdmann, J.R. Hörandel, T. Huege and J. Schulz, *Simulation of the Radiation Energy Release in Air Showers*, *EPJ Web Conf.* **135** (2017) 01016 [1609.05743].